Meng Law, MD
Amit M. Saindane, MD
Yulin Ge, MD
James S. Babb, PhD
Glyn Johnson, PhD
Lois J. Mannon, RT
Joseph Herbert, MD
Robert I. Grossman, MD

Index terms:
Brain, MR, 18.12144
Cerebral blood vessels, flow dynamics, 17.12144
Magnetic resonance (MR), perfusion study, 18.12144
Sclerosis, multiple, 18.871

Published online
10.1148/radiol.2313030996
Radiology 2004; 231:645–652

Abbreviations:
AIF = arterial input function
CBF = cerebral blood flow
CBV = cerebral blood volume
MS = multiple sclerosis
MTT = mean transit time
NAWM = normal-appearing white matter
ROI = region of interest
RR-MS = relapsing-remitting MS

[1] From the Departments of Radiology (M.L., A.M.S., Y.G., J.S.B., G.J., L.J.M., R.I.G.) and Neurology (J.H.), New York University Medical Center, MRI Department, Schwartz Building, Basement HCC, 530 First Ave, New York, NY 10016. Received June 24, 2003; revision requested September 3; revision received October 16; accepted November 12. Supported by National Institutes of Health grants RO1CA093992, NS29029, NCRR M01 RR00096 GCRC, and R37 NS 29029–11. **Address correspondence to** M.L. (e-mail: *lawm01@med.nyu.edu*).

Author contributions:
Guarantors of integrity of entire study, M.L., R.I.G.; study concepts, all authors; study design, M.L., Y.G., J.S.B., G.J., R.I.G.; literature research, M.L., A.M.S., Y.G.; clinical studies, M.L., Y.G., L.J.M., J.H.; data acquisition, M.L., Y.G., G.J., L.J.M.; data analysis/interpretation, all authors; statistical analysis, M.L., A.M.S., Y.G., J.S.B.; manuscript preparation, M.L., A.M.S., Y.G., J.S.B.; manuscript definition of intellectual content, M.L., Y.G., R.I.G.; manuscript editing, M.L., A.M.S., Y.G., G.J.; manuscript revision/review and final version approval, all authors

Microvascular Abnormality in Relapsing-Remitting Multiple Sclerosis: Perfusion MR Imaging Findings in Normal-appearing White Matter[1]

PURPOSE: To prospectively determine hemodynamic changes in the normal-appearing white matter (NAWM) of patients with relapsing-remitting multiple sclerosis (RR-MS) by using dynamic susceptibility contrast material–enhanced perfusion magnetic resonance (MR) imaging.

MATERIALS AND METHODS: Conventional MR imaging (which included acquisition of pre- and postcontrast transverse T1-weighted, fluid-attenuated inversion recovery, and T2-weighted images) and dynamic susceptibility contrast-enhanced T2*-weighted MR imaging were performed in 17 patients with RR-MS (five men and 12 women; median age, 38.4 years; age range, 27.6–56.9 years) and 17 control patients (seven men and 10 women; median age, 42.0 years; age range, 18.7–62.5 years). Absolute cerebral blood volume (CBV), absolute cerebral blood flow (CBF), and mean transit time (MTT) (referenced to an arterial input function by using an automated method) were determined in periventricular, intermediate, and subcortical regions of NAWM at the level of the lateral ventricles. Least-squares regression analysis (controlled for age and sex) was used to compare perfusion measures in each region between patients with RR-MS and control patients. Repeated-measures analysis of variance and the Tukey honestly significant difference test were used to perform pairwise comparison of brain regions in terms of each perfusion measure.

RESULTS: Each region of NAWM in patients with RR-MS had significantly decreased CBF ($P < .005$) and prolonged MTT ($P < .001$) compared with the corresponding region in control patients. No significant differences in CBV were found between patients with RR-MS and control patients in any of the corresponding areas of NAWM examined. In control patients, periventricular NAWM regions had significantly higher CBF ($P = .03$) and CBV ($P = .04$) than did intermediate NAWM regions. No significant regional differences in CBF, CBV, or MTT were found in patients with RR-MS.

CONCLUSION: The NAWM of patients with RR-MS shows decreased perfusion compared with that of controls.

Multiple sclerosis (MS) is a chronic inflammatory demyelinating disease of the central nervous system. The close relationship between MS lesions and the cerebral vasculature has long been recognized. Plaques are centered around small veins (1) and may extend along the axis of the vessel (2). At histopathologic examination, acute lesions show intense perivenular lymphocytic cuffing (3,4) that is associated with macrophage infiltration, demyelination, and axonal injury (5). Chronic lesions exhibit varying degrees of gliosis, oligodendrocyte depletion (6), and axonal loss (7). These plaques lack the perivenular

inflammation found in acute lesions (4,8) but often contain evidence of vascular injury such as thickening or hyalinization of vein walls (9).

It has become evident that the pathologic features in MS are far from limited to discrete lesions. Histopathologic and biochemical studies have revealed that areas of grossly normal-appearing white matter (NAWM) distant from lesions can exhibit loss of myelin-specific proteins (10), alterations in neurofilament phosphorylation (5), and infiltration by macrophages and T lymphocytes (11,12). Results obtained with advanced magnetic resonance (MR) imaging techniques such as proton MR spectroscopy (13–15) and magnetization transfer imaging (16–18) have supported the concept of the presence of diffuse pathologic features in areas of NAWM at conventional MR imaging.

Adams et al (9) described lymphocytic infiltration of vein walls without adjacent parenchymal inflammation, suggesting that MS represents a form of vasculitis that could precede lesion development. It has also been proposed that endothelial activation of cerebral vessels leads to vascular occlusion that precedes cerebral parenchymal inflammation and demyelination; this would indicate that MS represents an ischemic pathophysiologic process. Although changes in the microvasculature of NAWM cannot be demonstrated anatomically with conventional MR imaging, assessment of regional cerebral hemodynamics is possible by using dynamic susceptibility contrast material–enhanced T2*-weighted perfusion MR imaging. Perfusion MR imaging methods involve the utilization of signal changes that accompany the passage of a tracer through the cerebrovascular system and enable the quantitative estimation of cerebral blood flow and the mapping of regional variations in cerebral microvasculature. This technique has been used to demonstrate alterations in perfusion in a variety of pathologic intracranial processes, including neoplastic processes (20–22), acute ischemic stroke (23–25), and cerebral venous thrombosis (26).

A limited number of studies have involved evaluation of dynamic susceptibility contrast-enhanced MR imaging of MS lesions (27–30) by using a relative measure of cerebral blood volume (CBV); however, little is known about the hemodynamic changes in NAWM. Because the disease process in MS probably involves the entire brain, relative measures of CBV for which blood volume in the contralateral white matter or the deep gray structures is used as a reference could be problematic. Thus, the purpose of our study was to prospectively determine the hemodynamic changes in the NAWM of patients with relapsing-remitting MS (RR-MS) by using perfusion MR imaging.

MATERIALS AND METHODS

Patients with RR-MS and Control Patients

Approval for this study was obtained from the Institutional Board of Research Associates of New York University Medical Center, and informed consent was obtained from all patients. Seventeen consecutive patients with clinically definite RR-MS (31,32) met inclusion criteria for this study and were prospectively enrolled. There were five male patients (median age, 41.6 years; age range, 33.1–45.7 years) and 12 female patients (median age, 36.9 years; age range, 27.6–56.9 years). The median age of all 17 patients was 38.4 years (age range, 27.6–56.9 years), and the median duration of disease was 2.7 years (range, 0.2–17.0 years). Fourteen patients were undergoing immunomodulating therapy: 12 patients were receiving interferon β1-a (Avonex; Biogen, Cambridge, Mass), and two patients were receiving copolymer 1 (Copaxone; Teva, Petah Tiqvah, Israel); no patients received systemic corticosteroids during the study or in the 3 months preceding the study. These patients were examined by a board-certified neurologist (J.H.).

For comparison, 17 control patients were selected. These patients had no cerebrovascular disease or cardiovascular disease or evidence of small-vessel ischemic disease, ischemic stroke, or substantial intracranial disease at MR imaging. There were seven male patients (median age, 42.0 years; age range, 18.7–57.8 years) and 10 female patients (median age, 43.3 years; age range, 20.2–62.5 years). The median age of all 17 control patients was 42.0 years (age range, 18.7–62.5 years). Control patients were referred for MR imaging because of the following indications: headache ($n = 6$), to rule out stroke ($n = 5$), and to rule out intracranial mass ($n = 6$).

MR Imaging

Imaging was performed with a 1.5-T Vision MR imaging unit (Siemens Medical Systems, Malvern, Pa). Images were acquired by using our standard protocol for assessment of intracranial lesions. A localizing sagittal T1-weighted image was obtained; nonenhanced transverse T1-weighted (repetition time msec/echo time msec, 600/14), fluid-attenuated inversion recovery (9,000/110; inversion time, 2,500), intermediate-weighted (3,400/17), and T2-weighted (3,400/119) images were then acquired. A series of 60 gradient-echo echo-planar images were subsequently acquired at 1-second intervals during the first pass of a standard-dose (0.1 mmol per kilogram of body weight) bolus of gadopentetate dimeglumine (Magnevist; Berlex Laboratories, Wayne, NY). Seven 5-mm-thick sections were acquired. The sections were positioned (on the basis of findings on the T2-weighted images) to ensure coverage of a major vessel such as the anterior or middle cerebral arteries, the NAWM, and any lesions identified on the T2-weighted images.

All patients had an 18- or 20-gauge intravenous catheter placed in the antecubital fossa for the purpose of contrast material administration. The first 10 acquisitions were performed before contrast agent injection to establish a precontrast baseline. At the 10th acquisition, 0.1 mmol/kg of gadopentetate dimeglumine was injected with a power injector (Medrad, Pittsburgh, Pa) at a rate of 5 mL/sec. This was immediately followed by a bolus injection of saline (at 5 mL/sec to a total of 20 mL). The specific imaging parameters were as follows: 1,000/54; field of view, 230 × 230 mm; section thickness, 5 mm; matrix, 128 × 128; in-plane voxel size, 1.8 × 1.8 mm; intersection gap, 0%–30%; flip angle, 30°; and signal bandwidth, 1,470 Hz/pixel. The methods for acquiring perfusion data from a set of dynamic susceptibility contrast-enhanced echo-planar MR images have been previously described (21,33–35). Postcontrast transverse (600/14) T1-weighted images were obtained after acquisition of the perfusion data.

Image Processing and Evaluation

Data processing was performed off-line by using an Ultra 10 workstation (Sun Microsystems, Palo Alto, Calif) with programs developed in house (G.J.) by using the C and IDL (RSI, Boulder, Colo) programming languages. Absolute CBV, cerebral blood flow (CBF), and mean transit time (MTT) were calculated by using the method of Rempp et al (33,34). Briefly, tissue concentration is calculated from the change in relaxation rate that occurs during bolus passage. The tissue concentration that results from an idealized instantaneous bolus is then calculated by deconvolving the actual tissue concentration with the arterial input function (AIF). Deconvolution was performed

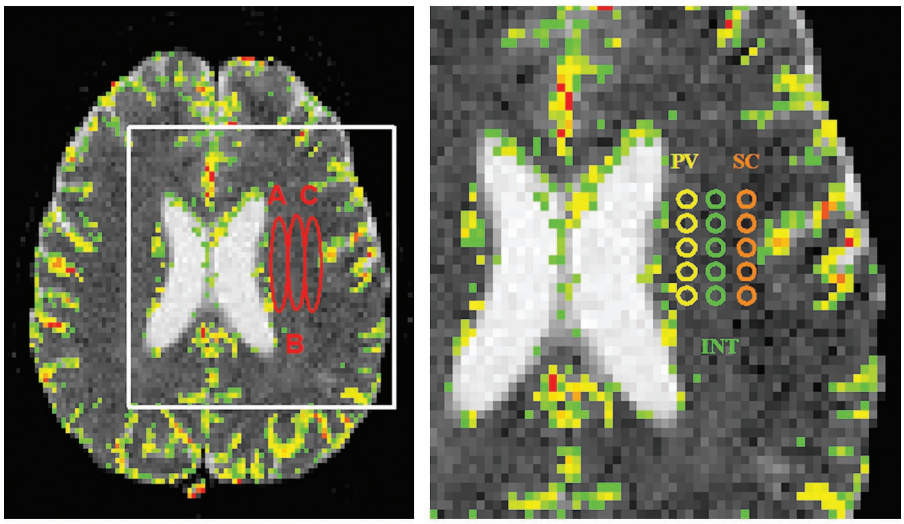

a. b.

Figure 1. **(a)** Transverse gradient-echo echo-planar MR image (1,000/54) with CBV map overlay shows the elliptical regions of NAWM that were examined: periventricular NAWM *(A)*, intermediate NAWM *(B)*, and subcortical NAWM *(C)*. In the perfusion color overlay map, areas of no color represent baseline white matter perfusion, green represents threshold gray matter perfusion, yellow represents increased perfusion, and red represents maximal perfusion. This is to ensure that ROIs are placed in the NAWM and lesions and vascular and gray matter structures are avoided. **(b)** Close-up of area in white box in **a**. To optimize reproducibility, five measurements were obtained from each of the three locations. These five CBV, CBF, and MTT measurements were recorded and averaged. ROIs were fixed in size (radius = 1 image pixel, 1.8 mm) and placed to avoid arterial or venous structures in NAWM, particularly in the periventricular and subcortical regions. Hence, each ROI has an in-plane resolution of 2 pixels. The location of ROI placement was at the same section position in patients with RR-MS and in control patients at the level of the ventricles. The ROIs were placed after visual coregistration with the transverse T2–weighted and fluid-attenuated inversion recovery MR images to ensure that lesions were not included in the ROI. *INT* = intermediate NAWM, *PV* = periventricular NAWM, *SC* = subcortical NAWM.

by using singular value decomposition (34,35).

During the first pass of the bolus of contrast agent, T2* is reduced, and, hence, the signal intensity on T2*-weighted images decreases. The change in relaxation rate (ΔR2*) (ie, the change in the reciprocal of T2*) can be calculated from the signal intensity with the following equation (36): $\Delta R2^*(t) = \{-\ln[SI(t)/SI_0]\}/TE$, where $SI(t)$ is the signal intensity at time t, SI_0 is the precontrast signal intensity, and TE is the echo time. ΔR2* is proportional to the concentration of contrast agent in the tissue, and CBV is proportional to the area under the curve of $\Delta R2^*(t)$, provided there is no recirculation or leakage of contrast agent (36).

In general, these assumptions are violated, but the effects can be reduced by fitting a gamma-variate function to the measured ΔR2* curve. This function approximates the curve that would have been obtained without recirculation or leakage. CBV can then be estimated from the area under the fitted curve rather than from the original data. Perfusion parameters are then calculated with the following equations:

$$\mathrm{MTT} = \frac{\int C_{\mathrm{dt}}}{C_{\max}},$$

$$\mathrm{CBV} = \frac{\int C_{\mathrm{dt}}}{\int \mathrm{AIF}_{\mathrm{dt}}},$$

and

$$\mathrm{CBF} = \frac{\mathrm{CBV}}{\mathrm{MTT}},$$

where C is the idealized tissue concentration found by using deconvolution, C_{dt} is C over time, $C_{\max}$ is the maximum value of C, and $\mathrm{AIF}_{\mathrm{dt}}$ is AIF over time. The AIF was calculated by using an automated method similar to that described by Rempp et al and Carroll et al (33,37). The maximal decrease in signal intensity, corresponding to the bolus peak, in each pixel within the head is obtained. The average signal intensity decrease and average bolus arrival time are then calculated for all pixels. Pixels in which the bolus arrives early and in which the signal intensity decrease is larger than average are assumed to be within arteries. The AIF is calculated by averaging the signal intensity values from all such pixels.

MTT, CBV, and CBF were calculated in regions of interest (ROIs) in three locations: periventricular NAWM, intermediate NAWM, and subcortical NAWM (Fig 1a). Intermediate NAWM was defined as the region of NAWM between the periventricular and the subcortical NAWM. To optimize reproducibility, five measurements were obtained from each of the three locations (Fig 1b), and these five CBV, CBF, and MTT measurements were recorded and averaged.

ROIs were fixed in size (radius = 1 image pixel, 1.8 mm) and were placed to avoid arterial or venous structures in NAWM, particularly in the periventricular and subcortical regions. Hence, each ROI had an in-plane resolution or diameter of 2 pixels. The location of ROI placement was at the same section position in patients and control patients at the level of the ventricles (Fig 1b). Within these section positions, the ROIs were placed in the same locations within the three regions described above.

The perfusion measurements were obtained by two authors (M.L. and Y.G.), who examined all cases in the study simultaneously to exclude interobserver and minimize intraobserver variation (38). Both authors had had more than 5 years of experience with this technique in clinical and research settings. To reduce the variability as to the location of ROI placement between patients, each patient data set was reviewed by both authors at the same time. Furthermore, the ROIs were placed after visual coregistration with the transverse T2-weighted and fluid-attenuated inversion recovery MR images to ensure that lesions were not included in the ROI.

Statistical Analysis

Least-squares regression analysis was used to compare patients with RR-MS and control patients with respect to the perfusion measures in each region after adjustment for differences attributable to age and sex was performed. A separate univariate analysis was performed for each perfusion measure. In each case, a Bonferroni correction was applied to adjust for the number of hypothesis tests conducted (one test for each of the three regions), and the model used to predict the perfusion measure was a linear function of patient age at the time of image acquisition and included a binary indicator of patient sex as a covariate.

For each of the two patient groups (ie, patients with RR-MS and control patients), repeated-measures analysis of variance (adjusted for age and sex) was used to compare the brain regions in terms of each perfusion measure, and the Tukey honestly significant difference test (adjusted for age and sex) was applied for pairwise comparison of brain regions in terms of each perfusion measure, while the experiment-wise type I error rate was maintained at or below the nominal 5% level. All significance levels reported below were calculated with two-sided tests and have been adjusted for the multiple hypothesis structure of the analysis (ie, by using a Bonferroni correction when comparing patients with RR-MS with control patients and the Tukey honestly significant difference test when comparing brain regions). *P* values less than .05 were considered to indicate statistically significant differences.

TABLE 1
Least-Squares Mean Values and SDs of Each Perfusion Measure (Adjusted for Sex and Age) in Each Region for Control Patients and Patients with RR-MS

Measure and Region	Control Patients*	Patients with RR-MS*	Adjusted *P* Value†
CBF			
Periventricular	34.84 ± 8.42	16.25 ± 9.49	<.0001
Intermediate	26.03 ± 11.78	14.01 ± 7.45	.004
Subcortical	31.25 ± 7.87	13.93 ± 8.34	<.001
CBV			
Periventricular	3.02 ± 1.14	2.61 ± 1.33	.260
Intermediate	2.11 ± 1.03	2.24 ± 1.49	.910
Subcortical	2.45 ± 0.99	2.13 ± 1.16	.291
MTT			
Periventricular	2.79 ± 0.88	6.14 ± 1.99	<.001
Intermediate	2.61 ± 0.98	6.44 ± 1.50	<.0001
Subcortical	2.67 ± 1.15	6.82 ± 2.22	<.0001

* Data are mean values ± SDs.
† *P* values for differences in values between patient groups were adjusted for multiple comparisons by using the Bonferroni method; $P < .05$ indicates a statistically significant difference.

RESULTS

No significant differences in mean or median age between control patients and patients with RR-MS were found ($P = .45$, unequal variance *t* test for comparison of means). However, the observed age difference could not be considered negligible: The difference in median age was 3.6 years, or 9.4% of the median age of patients. Consequently, subsequent analyses to compare data in patients with RR-MS and data in control patients were conducted both with and without inclusion of patient age and sex as covariates. The analyses performed with and without adjustment for age and sex produced identical results regarding statistical significance. The results presented are those obtained after adjustments were made for patient sex and age.

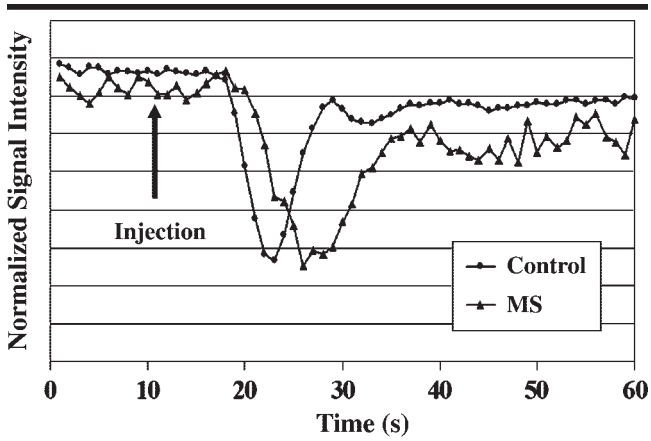

Figure 2. Graph shows signal intensity–versus-time curves measured in periventricular NAWM in a patient with RR-MS and a control patient. In both cases, injection of gadopentetate dimeglumine was performed at 10 seconds (arrow). The time to peak and MTT are significantly delayed ($P < .001$) in the patient with RR-MS, and the signal intensity curve is delayed and prolonged compared with the signal intensity curve for the control patient.

Comparison of Perfusion MR Imaging Measurements between Patients with RR-MS and Control Patients

After adjustment for sex and age, significant differences were found between control patients and patients with RR-MS with respect to CBF and MTT in each of the three regions of NAWM (periventricular, intermediate, and subcortical NAWM) (Table 1). There was a significant prolongation of MTT in patients with RR-MS compared with MTT in control patients: *P* values for comparison of MTT between patients with RR-MS and control patients in periventricular, intermediate, and subcortical NAWM were less than .001, less than .0001, and less than .0001, respectively. As an example, Figure 2 depicts the significant increase in MTT in the periventricular region of a patient with RR-MS compared with that in a control patient. There was a significant decrease in CBF in patients with RR-MS compared with CBF in control patients: *P* values for comparison of CBF between patients with RR-MS and control patients in periventricular, intermediate, and subcortical NAWM were less than .0001, .004, and less than .001, respectively. Figure 3 illustrates the significant decrease in CBF in periventricular, intermediate, and subcortical NAWM in patients with RR-MS compared with CBF in these areas in control patients. No significant differences were observed when CBV was compared between control patients and patients with RR-MS: *P* values were .260, .910, and .291 for periventricular, intermediate, and subcortical regions of NAWM, respectively.

Comparison of Perfusion MR Imaging Measurements between NAWM Regions

In the group of control patients, the Tukey honestly significant difference test revealed significant differences between periventricular NAWM and intermediate NAWM only. Specifically, the periventricular NAWM had significantly greater CBF and CBV than did the intermediate

TABLE 2
Results of Age- and Sex-adjusted Pairwise Comparison of NAWM Regions in Terms of Each Perfusion Measure

Perfusion Measure and Regions Compared	Control Patients		Patients with RR-MS	
	Difference between Least-Squares Means*	Adjusted *P* Value†	Difference between Least-Squares Means*	Adjusted *P* Value†
CBF				
Periventricular vs intermediate region	17.63	.03	4.47	.70
Periventricular vs subcortical region	7.18	.51	4.63	.69
Intermediate vs subcortical region	−10.44	.25	0.16	.99
CBV				
Periventricular vs intermediate region	0.91	.04	0.38	.69
Periventricular vs subcortical region	0.57	.28	0.48	.54
Intermediate vs subcortical region	−0.35	.61	0.11	.97
MTT				
Periventricular vs intermediate region	0.17	.87	−0.29	.89
Periventricular vs subcortical region	0.12	.93	−0.68	.55
Intermediate vs subcortical region	−0.05	.98	−0.38	.82

* Negative values indicate that the parameter in the first region was lower than that in the second region.

† *P* values were adjusted for multiple comparisons by using the Tukey honestly significant difference method with a family-wise type I error rate of 5%.

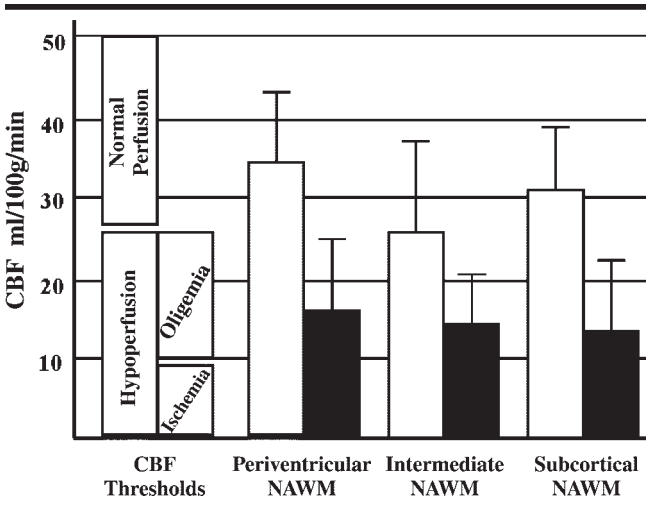

Figure 3. Bar graph illustrates the significant decrease in CBF in periventricular, intermediate, and subcortical NAWM in patients with RR-MS (black bars) compared with the CBF in these regions in control patients (white bars). Normal values and CBF threshold values for white matter hypoperfusion, oligemia, and ischemia (39) are shown on the left side of the graph. CBF values in the NAWM of patients with RR-MS are in the oligemic hypoperfusion range without being in the frankly ischemic range.

NAWM, with a progressive decline in perfusion from the periventricular NAWM to the subcortical NAWM; the intermediate NAWM had the lowest parameters. In the group of patients with RR-MS, there were no significant differences in CBF, CBV, or MTT between the three regions. The mean values for CBF, CBV, and MTT across the three regions are presented in Table 1. The significance levels resulting from the use of two tests to compare each perfusion measure pairwise across NAWM regions (ie, comparing periventricular, intermediate, and subcortical NAWM) in control patients and patients with RR-MS—as adjusted for age and sex—are presented in Table 2.

DISCUSSION

Dynamic susceptibility contrast-enhanced T2*-weighted echo-planar perfusion MR imaging is a robust and powerful tool for characterizing cerebral microvascular hemodynamics. In this study, we examined the NAWM at the level of the lateral ventricles and found reduced cerebral perfusion in patients with RR-MS compared with cerebral perfusion in control patients. In periventricular, intermediate, and subcortical regions of NAWM, CBF was significantly decreased and MTT was significantly prolonged. These results indicate that there is diffuse hemodynamic impairment throughout the NAWM of patients with RR-MS.

In all three regions of NAWM that we examined, the CBV was not significantly different in patients with RR-MS compared with that in control patients, suggesting that the degree of hypoperfusion is not sufficiently severe to cause significant ischemia or infarction. Results of a number of studies have demonstrated that CBV can be elevated or decreased depending on the level of hypoperfusion (40,41). White matter CBV can be elevated in some nonacute pathophysiologic states such as chronic unilateral carotid artery occlusion (42). In MS, as in other inflammatory diseases, vasodilation could be expected to occur because of perivascular inflammation, which in theory would increase CBV. However, since results of histopathologic studies have revealed that fibrin deposition and venous occlusive changes occur in MS lesions (19,43), the CBV in MS could remain unchanged owing to separate opposing effects from vascular inflammation and occlusion. In both settings (ie, inflammation and occlusion), CBF would be expected to decrease and MTT would be expected to increase. Additionally, it is likely that a modest reduction in CBF would stimulate autoregulatory mechanisms such as vasodilation and formation of collateral circulation in an attempt to increase CBF; this would tend to increase CBV and further prolong MTT (44,45). With further reductions in perfusion pressure, the capacity of autoregulatory vasodilatation would be overcome, and CBF and, eventually, CBV would then begin to decrease. At an extreme, further decreases in CBF would result in cerebral ischemia or infarction.

We interpret our findings of diminished perfusion in NAWM as evidence that MS has a primary vascular pathogenesis, and there is histopathologic evidence to support this hypothesis: Adams et al (9) described frequent edematous onion-skin changes and lymphocytic infiltration of vein walls in NAWM without adjacent parenchymal inflammation; this suggests

that MS represents a form of subacute or chronic vasculitis that could precede lesion development. Allen and McKeown (46) have also observed perivascular inflammation in areas of macroscopic NAWM.

In the present study, we found that control patients normally had significantly higher CBF and CBV in periventricular NAWM than in intermediate NAWM. This distinction was not present in the NAWM of patients with RR-MS, suggesting that there is a greater degree of perfusion abnormality in periventricular NAWM. This finding further supports the idea that MS has a vascular pathogenesis, since periventricular regions would be expected to be more prone to involvement with any process that selectively affects the cerebral microvasculature. Additional evidence for the idea of a primary vascular pathogenesis in MS comes from studies of patients with optic neuritis who developed MS. Lightman et al (47) found abnormalities such as fluorescein leakage and perivenous sheathing in retinal venules, a region free of myelin and oligodendrocytes. Arnold et al (48), in an autopsy study, found lymphocytic or granulomatous retinal periphlebitis in the absence of adjacent parenchymal inflammation, suggesting that vascular changes in MS can occur independently of contiguous demyelination or other parenchymal abnormalities.

There are several mechanisms by which a primary vascular disease process could lead to disease progression in MS. Given the close histopathologic relationship between MS lesions and cerebral veins (1,2) and the fact that central veins are almost invariably found in MS lesions at MR venography (49), it is possible that inflammation of cerebral veins in areas of NAWM could represent an early phase in the formation of acutely enhancing lesions. Chronic ischemia due to obliterative vasculitis could alternatively result in diffuse parenchymal dysfunction or damage.

Histopathologic evidence of vascular occlusion was described in the 1930s by Putnam (43), who suggested that vascular inflammation is a precursor of demyelination and may be a primary event in the evolution of the disease (50). Wakefield et al (19) later confirmed these findings in three acute cases of MS, demonstrating fibrin deposition and thrombosis of vessels in the absence of cellular infiltration and suggesting that thrombosis of small veins and capillaries could represent an ischemic basis for disease. Occlusive changes have also been clinically observed in the retinal venules of patients who later developed MS (51). Another mechanism could be the inflammatory cytokines produced by diffuse low-level inflammation of the cerebral veins of NAWM. For example, tumor necrosis factor α, which can be secreted by T lymphocytes and endothelial cells, is directly toxic to oligodendrocytes in culture (52) and causes demyelination of the optic nerve when it is administered directly into the vitreous chamber in mice (53).

Few previous imaging-based studies have involved examination of perfusion in MS. Lycke et al (54), who used single-photon emission computed tomography, reported significantly reduced regional CBF in the frontal gray matter of patients with progressive MS—but not patients with RR-MS—compared with regional CBF in control patients. One study involving perfusion MR imaging in nine patients with MS revealed that relative CBV compared with whole-brain CBV was significantly reduced in enhancing MS lesions versus nonenhancing lesions and NAWM (30). Another study of seven patients with RR-MS revealed decreased relative CBV in chronic lesions and further reduced relative CBV in one acute lesion compared with that in gray matter (29).

Haselhorst et al (27) examined 25 patients with MS and found that acute lesions had significantly higher relative CBV than NAWM and that chronic plaques had significantly lower relative CBV than NAWM. Cha et al (55) found large tumefactive demyelinating lesions to have prominent linear venous structures that are probably engorged periventricular veins. These lesions show reduced relative CBV at perfusion MR imaging. However, in both of these studies, CBV was examined relative to blood volume in contralateral white matter. Young et al (28) found that in one patient with MS, perfusion changes were seen beyond periventricular lesions, suggesting an abnormality of NAWM perfusion.

It is possible that decreased perfusion in NAWM could be related to widespread parenchymal damage in areas that cannot be seen with the spatial resolution at conventional MR imaging—damage that leads to a decreased metabolic demand for blood flow. Arguing against this are the histopathologic evidence that a primary vasculitis is involved and the greater involvement of highly vascular periventricular regions. Ultimately, it is unclear whether areas of abnormal perfusion are precursors of lesions, whether they occur independently of lesion development through a different mechanism, or whether they reflect decreased metabolic demand as a result of primary demyelination. It is also uncertain as to whether progressive subtypes of MS have different degrees of perfusion abnormality or whether qualitatively documenting a certain level of compromise in perfusion would help predict the natural history or progression of disease. Longitudinal studies and further investigation are required to address these questions.

Nonetheless, the vascular or ischemic basis for demyelination is intriguing. Provocation of symptoms in response to a hot bath, exercise, and food and alcohol intake are features of MS (56); similarly, experimental neural ischemia produces both conduction block and focal demyelination (57). All of these provocative stimuli share a common denominator—namely, vasodilatation of the extraneural vascular bed. Hence, despite autoregulation in regions of impaired perfusion, shunting of vascular reserve away from critically perfused regions in the central nervous system may trigger an acute deterioration. Although it has long been noted that there are vascular occlusive changes in MS (19), attention has been drawn to evidence in recent histopathologic studies of MS of hypoxia-like tissue injury (58).

The results of the present study raise the possibility of vascular involvement by the disease process in MS, and this possibility may eventually have an effect on the development and monitoring of new targets for therapy of MS. For example, results of recent studies have demonstrated that cholesterol-lowering statin drugs also have antiinflammatory effects that may be useful in the treatment of MS (59–61). It is also plausible that these drugs may not only aid in reducing inflammation in MS, but, through their cholesterol-lowering properties, may also have an effect on tissue perfusion by affecting the caliber of small vessels supplying the NAWM.

Although we believe that our findings in this study are substantial and have good pathophysiologic correlation, there were limitations inherent to the methodology. First, our comparative group of control patients, even though they did not have any cerebrovascular disease, cardiovascular disease, evidence of small vessel ischemic disease, ischemic stroke, or any marked intracranial pathology at MR imaging, did present for MR imaging with indications that may theoretically affect cerebral perfusion. It is important to note that six patients from the control group presented for investigation of headache, and perfusion abnormalities

have been reported in migraine (62). We are in the process of obtaining perfusion data in a group of healthy control subjects, and our preliminary data suggest that their perfusion parameters are similar to those of the control patients in the present study.

A second limitation was the effect of immunomodulating treatment (in 14 patients with RR-MS) on vascular permeability, vascular inflammation, and, possibly, vascular resistance. We are in the process of obtaining data in patients before and after immunomodulating therapy to assess for a possible effect of treatment on perfusion parameters.

A third limitation was that the perfusion algorithm is only accurate if there is negligible delay and dispersion in the bolus between the arteries in which the AIF is measured and the tissue of interest. The presence of delays and dispersion will introduce errors into the calculation of perfusion parameters (63,64). However, errors should have been minimized in the present study because the AIF was estimated close to the site of the perfusion measurements. Furthermore, there is no reason to believe that any dispersion we encountered would be significantly different between control patients and patients with MS. Dispersion would therefore only introduce a fixed error that would be similar in both patients with MS and control patients. AIF estimation can also be affected by partial volume effects and hematocrit levels (65).

Last, the effect of the disease process itself on the AIF is also not known, although at this time it seems that there is relative sparing of the major arteries in the vasculitic process (66) and, hence, the AIF may not be greatly affected in MS.

In summary, we believe that our finding of significantly reduced perfusion in the NAWM (ie, a prolonged MTT and a reduced CBF) of patients with RR-MS at dynamic susceptibility contrast-enhanced MR imaging raises the possibility of vascular involvement by the disease process in MS. We are aware of the current technical limitations with this technique, and, even though we must be cautious in not overinterpreting our findings, we will continue to investigate the role of dynamic susceptibility contrast-enhanced MR imaging in understanding MS and hope that our results will stimulate additional studies.

References

1. Dawson JW. The histology of disseminated sclerosis. Trans R Soc Edinb 1916; 108:397–399.
2. Fog T. On the vessel-plaque relationships in the brain in multiple sclerosis. Acta Neurol Scand 1964; 40(suppl 10):9–15.
3. Adams CW, Poston RN, Buk SJ. Pathology, histochemistry and immunocytochemistry of lesions in acute multiple sclerosis. J Neurol Sci 1989; 92:291–306.
4. Tanaka R, Iwasaki Y, Koprowski H. Ultrastructural studies of perivascular cuffing cells in multiple sclerosis brain. Am J Pathol 1975; 81:467–478.
5. Trapp BD, Peterson J, Ransohoff RM, Rudick R, Mork S, Bo L. Axonal transection in the lesions of multiple sclerosis. N Engl J Med 1998; 338:278–285.
6. Dowling P, Husar W, Menonna J, Donnenfeld H, Cook S, Sidhu M. Cell death and birth in multiple sclerosis brain. J Neurol Sci 1997; 149:1–11.
7. Ozawa K, Suchanek G, Breitschopf H, et al. Patterns of oligodendroglia pathology in multiple sclerosis. Brain 1994; 117: 1311–1322.
8. Adams CW. The onset and progression of the lesion in multiple sclerosis. J Neurol Sci 1975; 25:165–182.
9. Adams CW, Poston RN, Buk SJ, Sidhu YS, Vipond H. Inflammatory vasculitis in multiple sclerosis. J Neurol Sci 1985; 69: 269–283.
10. Trotter JL, Wegescheide CL, Garvey WF, Tourtellotte WW. Studies of myelin proteins in multiple sclerosis brain tissue. Neurochem Res 1984; 9:147–152.
11. Traugott U, Reinherz EL, Raine CS. Multiple sclerosis. Distribution of T cells, T cell subsets and Ia- positive macrophages in lesions of different ages. J Neuroimmunol 1983; 4:201–221.
12. Adams CW. Pathology of multiple sclerosis: progression of the lesion. Br Med Bull 1977; 33:15–20.
13. Narayanan S, Fu L, Pioro E, et al. Imaging of axonal damage in multiple sclerosis: spatial distribution of magnetic resonance imaging lesions. Ann Neurol 1997; 41:385–391.
14. Husted CA, Goodin DS, Hugg JW, et al. Biochemical alterations in multiple sclerosis lesions and normal-appearing white matter detected by in vivo 31P and 1H spectroscopic imaging. Ann Neurol 1994; 36:157–165.
15. Davie CA, Barker GJ, Thompson AJ, Tofts PS, McDonald WI, Miller DH. 1H magnetic resonance spectroscopy of chronic cerebral white matter lesions and normal appearing white matter in multiple sclerosis. J Neurol Neurosurg Psychiatry 1997; 63:736–742.
16. Filippi M, Campi A, Dousset V, et al. A magnetization transfer imaging study of normal-appearing white matter in multiple sclerosis. Neurology 1995; 45:478–482.
17. Loevner LA, Grossman RI, Cohen JA, Lexa FJ, Kessler D, Kolson DL. Microscopic disease in normal-appearing white matter on conventional MR images in patients with multiple sclerosis: assessment with magnetization-transfer measurements. Radiology 1995; 196:511–515.
18. Ge Y, Grossman RI, Udupa JK, Babb JS, Mannon LJ, McGowan JC. Magnetization transfer ratio histogram analysis of normal-appearing gray matter and normal-appearing white matter in multiple sclerosis. J Comput Assist Tomogr 2002; 26: 62–68.
19. Wakefield AJ, More LJ, Difford J, McLaughlin JE. Immunohistochemical study of vascular injury in acute multiple sclerosis. J Clin Pathol 1994; 47:129–133.
20. Aronen HJ, Gazit IE, Louis DN, et al. Cerebral blood volume maps of gliomas: comparison with tumor grade and histologic findings. Radiology 1994; 191:41–51.
21. Knopp EA, Cha S, Johnson G, et al. Glial neoplasms: dynamic contrast-enhanced T2*-weighted MR imaging. Radiology 1999; 211:791–798.
22. Sugahara T, Korogi Y, Kochi M, et al. Correlation of MR imaging-determined cerebral blood volume maps with histologic and angiographic determination of vascularity of gliomas. AJR Am J Roentgenol 1998; 171:1479–1486.
23. Thijs VN, Adami A, Neumann-Haefelin T, Moseley ME, Albers GW. Clinical and radiological correlates of reduced cerebral blood flow measured using magnetic resonance imaging. Arch Neurol 2002; 59: 233–238.
24. Smith AM, Grandin CB, Duprez T, Mataigne F, Cosnard G. Whole brain quantitative CBF, CBV, and MTT measurements using MRI bolus tracking: implementation and application to data acquired from hyperacute stroke patients. J Magn Reson Imaging 2000; 12:400–410.
25. Sorensen AG, Copen WA, Ostergaard L, et al. Hyperacute stroke: simultaneous measurement of relative cerebral blood volume, relative cerebral blood flow, and mean tissue transit time. Radiology 1999; 210:519–527.
26. Doege CA, Tavakolian R, Kerskens CM, et al. Perfusion and diffusion magnetic resonance imaging in human cerebral venous thrombosis. J Neurol 2001; 248: 564–571.
27. Haselhorst R, Kappos L, Bilecen D, et al. Dynamic susceptibility contrast MR imaging of plaque development in multiple sclerosis: application of an extended blood-brain barrier leakage correction. J Magn Reson Imaging 2000; 11:495–505.
28. Young IR, Hall AS, Bryant DJ, et al. Assessment of brain perfusion with MR imaging. J Comput Assist Tomogr 1988; 12: 721–727.
29. Jensen CV, Rostrup E, Blinkenberg M, Larsson HBW, Henriksen O. Relative regional cerebral blood volume in multiple sclerosis (abstr). In: Proceedings of the Society of Magnetic Resonance in Medicine and the European Society of Magnetic Resonance in Medicine and Biology. Berkeley, Calif: Society of Magnetic Resonance in Medicine, 1995; 1297.
30. Petrella JR, Yang Y, Richert N, et al. Dynamic contrast MR measurements of relative cerebral blood volume in enhancing multiple sclerosis lesions: comparison to nonenhancing lesions and normal appearing white matter (abstr). In: Proceedings of the Fifth Meeting of the International Society for Magnetic Resonance in Medicine. Berkeley, Calif: International Society for Magnetic Resonance in Medicine, 1997; 646.
31. Poser CM, Paty DW, Scheinberg L, et al. New diagnostic criteria for multiple sclerosis: guidelines for research protocols. Ann Neurol 1983; 13:227–231.
32. Lublin FD, Reingold SC. Defining the

clinical course of multiple sclerosis: results of an international survey. National Multiple Sclerosis Society (USA) Advisory Committee on Clinical Trials of New Agents in Multiple Sclerosis. Neurology 1996; 46:907–911.
33. Rempp KA, Brix G, Wenz F, Becker CR, Guckel F, Lorenz WJ. Quantification of regional cerebral blood flow and volume with dynamic susceptibility contrast-enhanced MR imaging. Radiology 1994; 193:637–641.
34. Ostergaard L, Sorensen AG, Kwong KK, Weisskoff RM, Gyldensted C, Rosen BR. High resolution measurement of cerebral blood flow using intravascular tracer bolus passages. II. Experimental comparison and preliminary results. Magn Reson Med 1996; 36:726–736.
35. Ostergaard L, Weisskoff RM, Chesler DA, Gyldensted C, Rosen BR. High resolution measurement of cerebral blood flow using intravascular tracer bolus passages. I. Mathematical approach and statistical analysis. Magn Reson Med 1996; 36:715–725.
36. Rosen BR, Belliveau JW, Vevea JM, Brady TJ. Perfusion imaging with NMR contrast agents. Magn Reson Med 1990; 14:249–265.
37. Carroll TJ, Rowley HA, Haughton VM. Automatic calculation of the arterial input function for cerebral perfusion imaging with MR imaging. Radiology 2003; 227:593–600.
38. Wetzel SG, Cha S, Johnson G, et al. Relative cerebral blood volume measurements in intracranial mass lesions: interobserver and intraobserver reproducibility study. Radiology 2002; 224:797–803.
39. Schlaug G, Benfield A, Baird AE, et al. The ischemic penumbra: operationally defined by diffusion and perfusion MRI. Neurology 1999; 53:1528–1537.
40. Karonen JO, Vanninen RL, Liu Y, et al. Combined diffusion and perfusion MRI with correlation to single-photon emission CT in acute ischemic stroke: ischemic penumbra predicts infarct growth. Stroke 1999; 30:1583–1590.
41. Hatazawa J, Shimosegawa E, Toyoshima H, et al. Cerebral blood volume in acute brain infarction: a combined study with dynamic susceptibility contrast MRI and 99mTc-HMPAO-SPECT. Stroke 1999; 30: 800–806.
42. Kluytmans M, van der Grond J, Folkers PJ, Mali WP, Viergever MA. Differentiation of gray matter and white matter perfusion in patients with unilateral internal carotid artery occlusion. J Magn Reson Imaging 1998; 8:767–774.
43. Putnam TJ. Evidences of vascular occlusion in multiple sclerosis and encephalomyelitis. Arch Neurol Neuropsychol 1935; 32:1298–1321.
44. Grandin CB, Duprez TP, Smith AM, et al. Which MR-derived perfusion parameters are the best predictors of infarct growth in hyperacute stroke? comparative study between relative and quantitative measurements. Radiology 2002; 223:361–370.
45. Sorensen AG, Reimer P. Cerebral perfusion imaging principles and current applications. New York, NY: Thieme, 2000.
46. Allen IV, McKeown SR. A histological, histochemical and biochemical study of the macroscopically normal white matter in multiple sclerosis. J Neurol Sci 1979; 41:81–91.
47. Lightman S, McDonald WI, Bird AC, et al. Retinal venous sheathing in optic neuritis: its significance for the pathogenesis of multiple sclerosis. Brain 1987; 110:405–414.
48. Arnold AC, Pepose JS, Hepler RS, Foos RY. Retinal periphlebitis and retinitis in multiple sclerosis. I. Pathologic characteristics. Ophthalmology 1984; 91:255–262.
49. Tan IL, van Schijndel RA, Pouwels PJ, et al. MR venography of multiple sclerosis. AJNR Am J Neuroradiol 2000; 21:1039–1042.
50. Putnam TJ. The pathogenesis of multiple sclerosis: a possible vascular factor. N Engl J Med 1933; 209:786–790.
51. Graham EM, Stanford MR, Sanders MD, Kasp E, Dumonde DC. A point prevalence study of 150 patients with idiopathic retinal vasculitis. I. Diagnostic value of ophthalmological features. Br J Ophthalmol 1989; 73:714–721.
52. Selmaj KW, Raine CS. Tumor necrosis factor mediates myelin and oligodendrocyte damage in vitro. Ann Neurol 1988; 23: 339–346.
53. Jenkins HG, Ikeda H. Tumour necrosis factor causes an increase in axonal transport of protein and demyelination in the mouse optic nerve. J Neurol Sci 1992; 108:99–104.
54. Lycke J, Wikkelso C, Bergh AC, Jacobsson L, Andersen O. Regional cerebral blood flow in multiple sclerosis measured by single photon emission tomography with technetium-99m hexamethylpropyleneamine oxime. Eur Neurol 1993; 33:163–167.
55. Cha S, Pierce S, Knopp EA, et al. Dynamic contrast-enhanced T2*-weighted MR imaging of tumefactive demyelinating lesions. AJNR Am J Neuroradiol 2001; 22: 1109–1116.
56. Halliday AM, McDonald WI. Pathophysiology of demyelinating disease. Br Med Bull 1977; 33:21–27.
57. Gibson GE, Shimada M, Blass JP. Alterations in acetylcholine synthesis and cyclic nucleotides in mild cerebral hypoxia. J Neurochem 1978; 31:757–760.
58. Lassmann H. Hypoxia-like tissue injury as a component of multiple sclerosis lesions. J Neurol Sci 2003; 206:187–191.
59. Neuhaus O, Strasser-Fuchs S, Fazekas F, et al. Statins as immunomodulators: comparison with interferon-beta 1b in MS. Neurology 2002; 59:990–997.
60. Zamvil SS, Steinman L. Cholesterol-lowering statins possess anti-inflammatory activity that might be useful for treatment of MS (editorial). Neurology 2002; 59:970–971.
61. Youssef S, Stuve O, Patarroyo JC, et al. The HMG-CoA reductase inhibitor, atorvastatin, promotes a Th2 bias and reverses paralysis in central nervous system autoimmune disease. Nature 2002; 420: 78–84.
62. Cutrer FM, Sorensen AG, Weisskoff RM, et al. Perfusion-weighted imaging defects during spontaneous migrainous aura. Ann Neurol 1998; 43:25–31.
63. Calamante F, Gadian DG, Connelly A. Delay and dispersion effects in dynamic susceptibility contrast MRI: simulations using singular value decomposition. Magn Reson Med 2000; 44:466–473.
64. Calamante F, Gadian DG, Connelly A. Quantification of perfusion using bolus tracking magnetic resonance imaging in stroke: assumptions, limitations, and potential implications for clinical use. Stroke 2002; 33:1146–1151.
65. Axel L. Cerebral blood flow determination by rapid-sequence computed tomography: theoretical analysis. Radiology 1980; 137:679–686.
66. Adams CW. Vascular aspects of multiple sclerosis. In: Adams CW, ed. A colour atlas of multiple sclerosis and other myelin disorders. 1st ed. London, England: Wolfe, 1989; 184–188.